08,10

Nanostructuring of the surface of Bi_2Te_3 epitaxial films during ion-plasma treatment

© S.P. Zimin[1,2], I.I. Amirov[1], V.V. Naumov[1], M.S. Tivanov[3], L.S. Lyashenko[3], O.V. Korolik[3], E. Abramof[4], P.H.O. Rappl[4]

[1] Valiev Institute of Physics and Technology of RAS, Yaroslavl Branch,
Yaroslavl, Russia
[2] Demidov State University,
Yaroslavl, Russia
[3] Belarusian State University,
Minsk, Republic of Belarus
[4] Materials and plasma research and development group (GPDMP), National Institute for Space Research (INPE),
São José dos Campos, 12227-010, Brazil

E-mail: zimin@uniyar.ac.ru

Received May 20, 2024
Revised June 6, 2024
Accepted June 10, 2024

The effect of ion plasma treatment on the surface morphology and optical properties of Bi_2Te_3 epitaxial films has been studied. Bismuth telluride films were grown by molecular beam epitaxy on (111)BaF_2 substrates and had a thickness of 290 nm. Ion-plasma treatment of the film surface was carried out in a high-density argon plasma reactor with a high-frequency induction discharge (13.56 MHz) and low pressure. The energy of Ar^+ ions was set in the range of 25−150 eV, the duration of treatment was in the range of 10−120 s. Effective nanostructuring of the surface of bismuth telluride was discovered, leading to the appearance of nanostructures of various shapes and architectures with geometric sizes of 13−40 nm. From the optical transmission spectra, the value of the band gap $E_g = 0.87-1.29$ eV for nanostructured Bi_2Te_3 systems was determined. The obtained E_g values are several times higher than the values for bulk bismuth telluride (~ 0.16 eV), which can be explained by the implementation of quantum size effects.

Keywords: bismuth telluride, epitaxial films, ion-plasma treatment, nanostructures, Raman scattering, reflection and transmission spectra.

DOI: 10.61011/PSS.2024.08.59060.131

1. Introduction

Bismuth telluride (Bi_2Te_3) is semiconductor compound of group $A_2^VB_3^{VI}$, has small band gap ~ 0.16 eV, and was widely used in thermoelectric devices for more than half a century [1]. The crystalline structure Bi_2Te_3 is layered, consisting of quintuple layers Te^1-Bi-Te^2-Bi-Te^1 with internal covalent bonds and weak Van der Waals bonds between quintuple layers. Detection in bismuth telluride of the topological insulator properties [2–4], Increased during last years interest to unique properties of layered 2D materials [5,6] predetermined new directions of study Bi_2Te_3, associated with formation of low-dimensional systems and instrumentation devices based on them. This improves not only parameters of the thermoelectric devices, but suggest areas of practical application of the bismuth telluride in electronics, optoelectronics, in materials science of microwave absorbers etc. [6–12].

For surface modification of bulk and film samples of Bi_2Te_3 and its provision with set morphological and structural properties, the authors of various works used technological methods, including pulsed photon processing [13], femtosecond laser effect [14], electron irradiation [15], thermal annealing [16–18] etc. It is known [19], this method of ion-plasma treatment is rather effective to form surface of solid bodies with required parameters, from its planarization and to the creation of ensembles of nanostructures of various architectures. Currently several papers [20,21] are known relating the method of ion-plasma treatment application to samples of bismuth telluride. The present paper task was study of processes of surface nanostructuring of epitaxial films of Bi_2Te_3 on substrates of barium fluoride during treatment in argon plasma with different parameters. The relevance of the studies conducted is also associated with the lack of experimental and theoretical information about the features of the physical processes occurring during the interaction of ions with the surface of layered 2D materials [22,23].

2. Experimental part

Films of bismuth telluride were grown on fresh chipped substrates (111) BaF_2 with size $15 \times 15\,mm^2$ by method of molecular-beam epitaxy using Riber 32P MBE system comprising effusion cells Bi_2Te_3 and Te. The method of film growth is described in detail in paper [24]. Barium fluoride

selection as substrate is due to the fact that triangular atomic pattern of its surface, coinciding with the plane (111) of cube lattice BaF_2, practically coincides with the atomic pattern of plane (001) of hexagonal lattice Bi_2Te_3. At distance between atoms 4.384 Å mismatch of lattices is about 0.04%, this ensures ideal conditions for the epitaxy. The grown film thickness was 290 nm. Additional studies by method of X-ray diffractometry [24,25] showed high structural perfection of the grown films with the implementation of epitaxial growth, in which (001) hexagonal planes Bi_2Te_3 were parallel to surface (111) BaF_2. All samples, as thermoprobe measurements showed, had *p*-type of conductivity.

The ion-plasma treatment of film surfaces of bismuth telluride was performed in a reactor of high-density argon plasma of low-pressure high-frequency induction discharge (13.56 MHz). The treatment modes were as follows: argon flowrate was 20 sccm, working pressure in the reactor was 0.14 Pa, RF-power on the inductor was 800 W, RF-bias power on the aluminum substrate holder varied in range 0–80 W. Average energy (E_i) of ions Ar^+, determined by value of displacement RF-power, was set in range 25–150 eV. Density of ion current upon displacement power change did not change and was $5.2\,mA \cdot cm^{-2}$. The duration of ion-plasma treatment (t) was in the range 10–120 s.

The surface morphology was studied by scanning electron microscopy (SEM) using Supra 40 (Carl Zeiss) unit in the mode of secondary electron recording (InLens). Local chemical analysis was carried out using an energy-dispersive X-ray (EDX) analysis attachment INCA Energy (Oxford Instruments).

The Raman scattering (RS) spectra were measured by spectrometer with confocal microscope Nanofinder HE (LOTIS TII). The excitation was implemented by a solid-state laser 532 nm in continuous mode with an optical power of $\sim 60\,\mu W$. The laser radiation was focused onto the sample surface into a spot with a diameter of $\sim 0.7\,\mu m$. The backscattered light was dispersed by a $600\,mm^{-1}$ diffraction grating, which allowed for a spectral resolution of not worse than $3\,cm^{-1}$. The photodetector was a cooled silicon CCD-matrix, the signal accumulation time was 30 s.

Spectra of optical transmittance and specular reflection were registered using spectrophotometer Photon RT (EssentOptics) in unpolarized light with a spectral resolution of at least 5 nm in the wavelength range 200–2500 nm. The specular reflection spectra were registered during incidence of optical radiation on the surface of the sample at an angle of 8° to the normal. The size of optical incident beam on the surface under study was about $4.5 \times 4.5\,mm^2$.

3. Results and discussion

Figure 1 shows typical images of film surfaces of bismuth telluride in initial state. The surface morphology was characterized by presence of elevations and depressions of a triangular shape with submicron dimensions at the base, comprising steps-terraces of nanometer height. Such surface pattern is typical for epitaxial pair Bi_2Te_3/BaF_2 (111) [26,27], the physical models of steps-terraces occurrence are discussed in detail in papers [28–30]. Note that formation of such step structures is natural for heteroepitaxial films and other layered semiconductors [31].

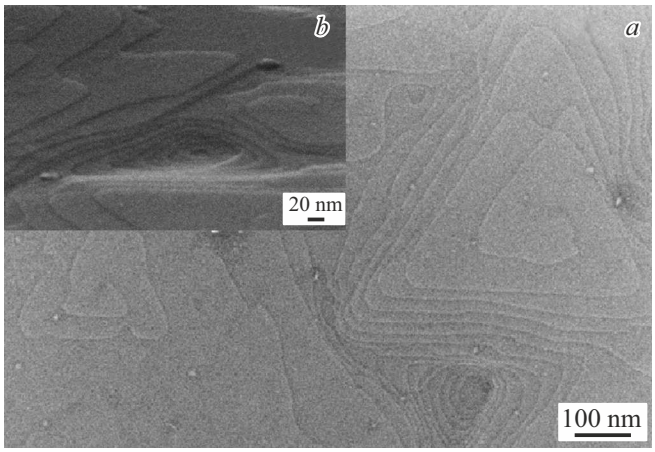

Figure 1. SEM-images of film surface of bismuth telluride in initial state during shooting along normal to surface (*a*) and deviation from normal by 70° (*b*).

The first experiments on ion-plasma sputtering of bismuth telluride films shown a unique response of the material to bombardment of the surface with argon ions. It was identified that sputtering rates Bi_2Te_3 are abnormally high as compared with other classic materials of electronics. In range of used energies of ions 25–150 eV the sputtering rates increase linearly from 1.2 to $20\,nm \cdot s^{-1}$, this exceeds the sputtering rates (at similar experiment conditions) for lead chalcogenides PbTe, PbSe, PbS, which are among leaders in semiconductors in terms of the sputtering rates. For ions energy 150 eV upon recalculation to density of ion flow $1\,mA \cdot cm^{-2}$ the sputtering rate of bismuth telluride was $3.8\,nm \cdot s^{-1}$. This value by almost 2 times exceeds the sputtering rate of lead chalcogenides ($1.6–1.9\,nm \cdot s^{-1}$) and by several times is higher the rates for Si, InN, GaN, InSb and GaAs ($0.02–0.7\,nm \cdot s^{-1}$) [32]. From a physical point of view, the obtained result can be explained by the layered structure of bismuth telluride with weak Van der Waals interaction between the quintuple layers. The same effect was described by us previously for crystals of layered semiconductor GaTe in [33].

3.1. Morphology of film surface of bismuth telluride after treatment by argon ions

High values of sputtering rates for films Bi_2Te_3 abruptly decrease the technology possibilities of modes variation of plasma treatment, providing for experiments at fixed density of ion flow the compromise of small value of ion energies and small duration of processes. Figures 2

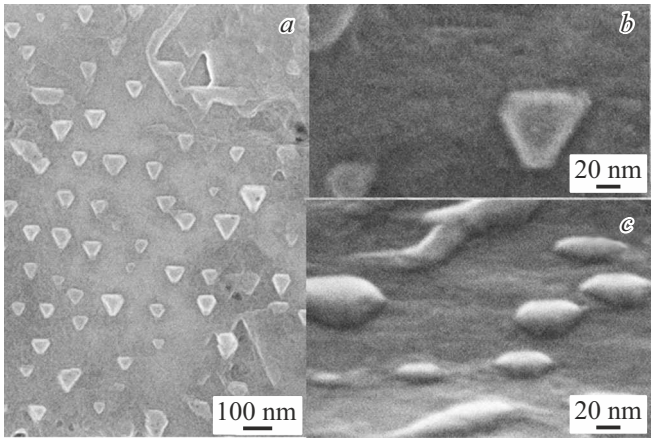

Figure 2. Morphology of film surfaces of bismuth telluride after treatment by ions with energy 25 eV, 90 s. *a, b* — shooting along normal to surface, *c* — during deviation from normal by 70°.

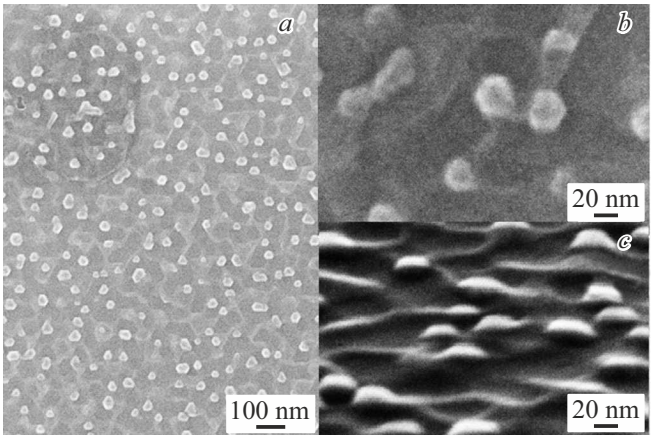

Figure 3. Morphology of film surfaces of bismuth telluride after treatment by ions with energy 25 eV, 120 s. *a, b* — shooting along normal to surface, *c* — during deviation from normal by 70°.

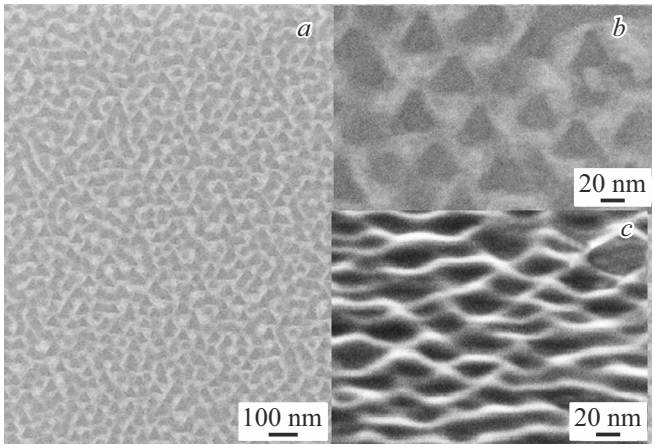

Figure 4. SEM-images of film surface of bismuth telluride after treatment with argon ions $E_i = 50$ eV, $t = 40$ s. *a, b* — shooting along normal to surface, *c* — during deviation from normal by 70°.

and 3 show images of film surface of bismuth telluride after treatment with argon ions at minimum possible ion energy 25 eV at process duration 90 and 120 s. Figures show that treatment resulted in effective nanostructuring of surface. At process duration $t = 90$ s (Figure 2) on surface the homogeneous ensemble of quasi-flat triangular nanostructures was formed. Lateral dimensions of side of equilateral triangle were 60 ± 10 nm, the surface density was in range $(3-4) \cdot 10^9\,\mathrm{cm}^{-2}$. Nanostructure height were 20 ± 5 nm, sides of all triangles were ordered along several directions, corresponding to the surface crystalline structure. At $t = 120$ s (Figure 3) the situation changed — at background of disappearance of the clear faceting of nanostructures, there was a sharp increase in their surface density to $(1-2) \cdot 10^{10}\,\mathrm{cm}^{-2}$, the lateral dimensions decreased to 25 ± 5 nm, height did not exceed 20 nm.

Upon increase in ion energy to 50 eV the surface morphology continued its changes. Figure 4 shows the morphology of film surface of bismuth telluride after treatment by argon ions with energy 50 eV for 40 s. Photos show that ensemble of triangular nanoregions is formed, they are separated by elevations with height up to 20 nm. Triangular pits are equilateral with the side dimensions 40 ± 10 nm, their surface density is $(4-5) \cdot 10^{10}\,\mathrm{cm}^{-2}$, the sides of the triangles are equally oriented in the plane of the film. In terms of general view on the formed pattern we can say about formation of quasi-homogeneous wavy surface with lateral size of about 60 nm.

Energy increasing of argon ions to 100 eV, amended by mandatory condition to decrease the process duration resulted in the formation of more shallow in lateral direction homogeneous nanorelief. The surface morphology for treatment conditions $E_i = 100$ eV, $t = 10$ s is given in Figure 5. On surface the homogeneous ensemble of hemispherical structures whose lateral dimensions and the distances between the edges of the hemispheres did not exceed 20 nm.

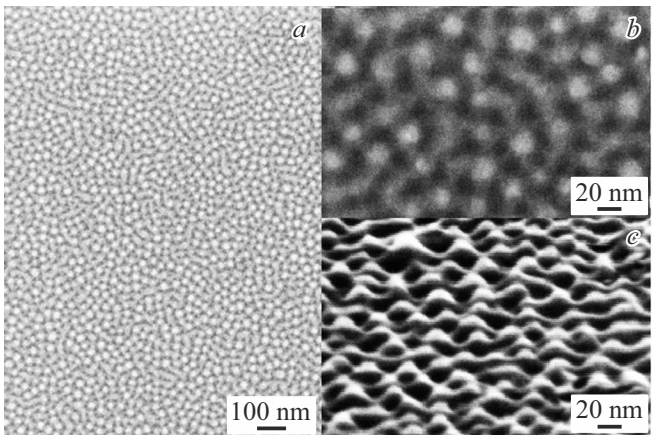

Figure 5. Morphology of surface Bi_2Te_3 after bombardment by argon ions with energy 100 eV for 10 s. *a, b* — shooting along normal to surface, *c* — at deviation from normal by 70°.

To understand the overall picture of the processes occurring at the initial stage of ion-plasma treatment, additional studies were conducted related to the study of the influence of the ion energy value E_i on surface morphology of films Bi_2Te_3 at low treatment times. The ion energy in experiment varied in range 50–150 eV, treatment duration was same and equal to $t = 10$ s. Results of these studies are given in Figure 6. The surface morphology did not depend on ion energy, and pattern of the observed nanorerief was practically identical to described in Figure 5 case for $E_i = 100$ eV, $t = 10$ s. This states that the initial physical processes of nanorelief formation for the applied range of ion energies are the same, and subsequent changes in the creation of nanostructures with different sizes and shapes are determined by different temperature modes depending on the ion energy and the process duration.

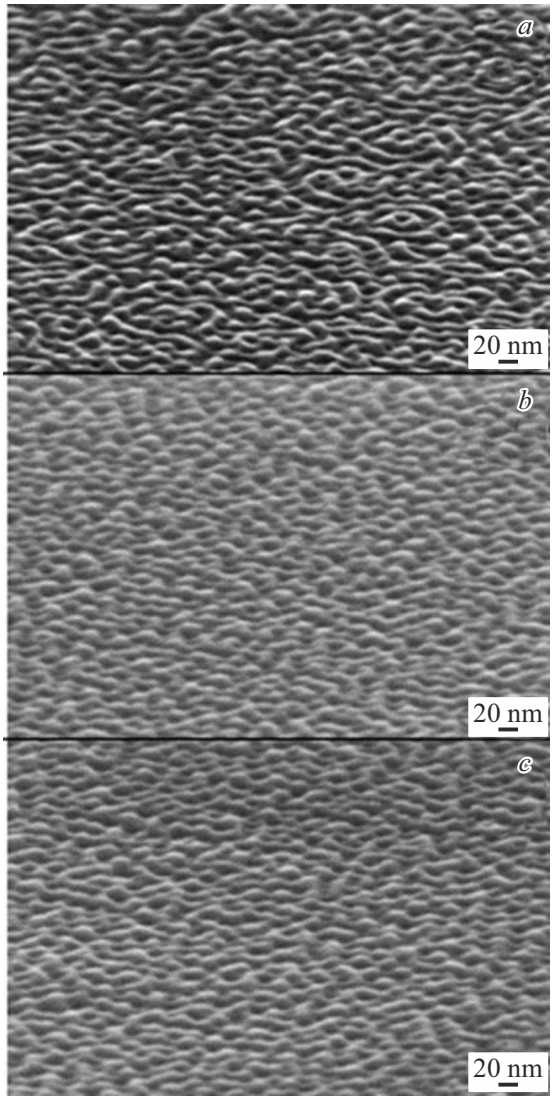

Figure 6. SEM-images of film surfaces of bismuth telluride after sputtering with argon ions with energy 50 eV (*a*), 125 eV (*b*), 150 eV (*c*) for 10 s. Shooting was performed at deviation from normal by 70°.

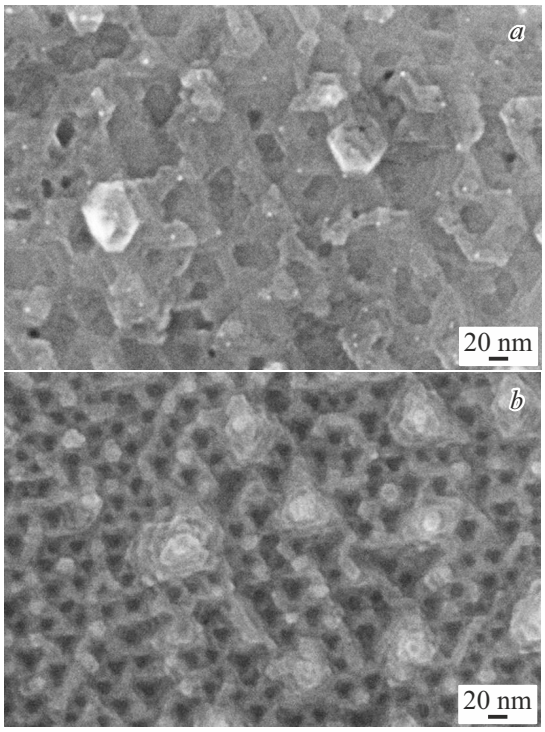

Figure 7. Morphology of film surface of bismuth telluride after two-step treatments: $E_i = 25$ eV, $t = 120$ s + $E_i = 50$ eV, $t = 10$ s (*a*), $E_i = 25$ eV, $t = 90$ s + $E_i = 100$ eV, $t = 10$ s (*b*).

During studies we determined additional possibilities in surface nanostructuring of bismuth telluride during successive ion-plasma treatments under various modes. Some examples of formed nanorelief as result of two-step treatments are given in Figure 7, they show that implementation of these conditions increases variety of shapes and dimensions of the formed ensembles of nanostructure on surface of bismuth telluride. Note that observed during ion-plasma treatment nanostructures of triangular and hexagonal shape are typical during creation of nanostructures on surface Bi_2Te_3 and are explained by structural features of crystal lattice of bismuth telluride [34–37].

3.2. Chemical composition of surface, data of RS spectroscopy

EDX analysis was used to study possible changes of chemical composition of film surface of bismuth telluride after plasma treatments. Measurements were performed at voltage 6 kV and sample inclination to angle 70°, this increased ration of signals „surface/volume“ and described more accurately the chemical composition on surface [33]. In initial state content of tellurium and bismuth at different regions of surface was 61.83 ± 0.10 and 38.17 ± 0.10 at.%. After the ion-plasma treatment in all above described modes the result was the same — chalcogen content decreased, and metal content increased. These changes were small, did not exceed for each chemical element 3–4 at.%, but

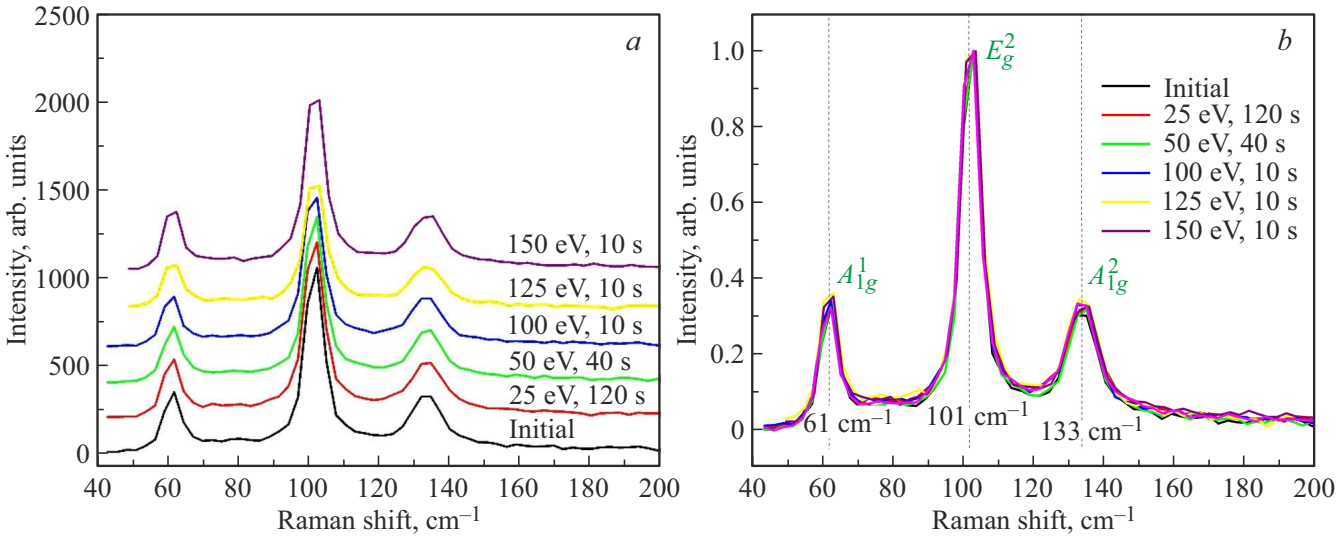

Figure 8. RS spectra Bi_2Te_3 before and after treatment in argon plasma at excitation 532 nm before (*a*) and after normalization to the maximum signal (*b*).

consistently confirmed enrichment of the surface with metal atoms. Application for theoretical analysis of the known formulas for the case of binary compounds within the framework of linear cascade theory [33,38] showed that ratio of partial coefficients of sputtering of tellurium and bismuth in the studied case is 2.4, this shall result in prevailing sputtering of tellurium in two-component material and surface enrichment by metal.

RS spectra of volume Bi_2Te_3 is characterized [39,40] by presence of peaks $E_g^1, A_{1g}^1, E_g^2, A_{1g}^2 \sim 35, 61, 101, 132\,\text{cm}^{-1}$. In our case the peak E_g^1 is not observed, because it is not passed by the edge filter. The peaks A_{1g}^1, E_g^2, A_{1g}^2 were registered in all samples Bi_2Te_3 both before and after plasma treatments (Figure 8, *a*). When RS spectra are excited by laser with wavelength 532 nm (60 μW, 30 s) position, width at half maximum, and ratio of peak intensities A_{1g}^2 and E_g^2 did not change (Figure 8, *b*). The same result was obtained by the authors of the article [20] when processing bismuth telluride flakes with a thickness of 100 nm in argon plasma.

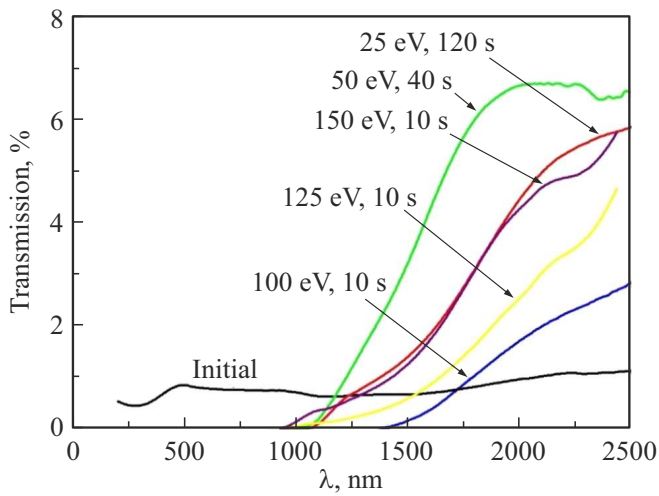

Figure 9. Spectra of optical transmittance of films Bi_2Te_3 before and after treatment in argon plasma.

3.3. Optical characteristics

Determined by experiments spectral dependencies of reflectance R and transmittance T are given in Figures 9 and 10 respectively. For initial sample the transmittance in all studied spectral range is practically constant and is about one percent. For plasma treated films Bi_2Te_3 in region 1000−1500 nm we observed abrupt increase in transmittance (Figure 9), natural for edge of intrinsic absorption of semiconductor materials.

Value of reflectance for the initial film Bi_2Te_3 for $\lambda > 500$ nm achieves plateau and is 20%. For all films after plasma treatment the increase in reflectivity was observed. Maximum value of reflectance at level of 60% corresponded to ion energies 125 and 150 eV for 10 s.

In spectrum of specular optical reflection (Figure 11) we can separate several clear peaks A_1–A_6, described in [41]. Peak A_1 is closer to edge of absorption; tip of basic wide maximum comprises two peaks A_2 and A_3, shortwave portion of maximum is formed by group of peaks $A_{4,5}$, A_6. Energy positions of peaks of reflectivity A_1–A_6 of films Bi_2Te_3 are shown in Table 1.

In region from 1 to 4 eV there is one of main maxima of reflectivity containing triplet structure [42]. The observed peaks of triplet are designated as E_1, E_2, E_3. In paper [42] the supposition was made that triplet structure was due to spin-orbit splitting, and electronic transition responsible for peaks E_1, E_2, E_3, occur in point Γ (center of Brillouin zone).

Table 1. Energy positions of peaks A_1-A_6 of surface reflectivity of films Bi_2Te_3

Modes of treatment	Initial state	25 eV, 120 s	50 eV, 40 s	100 eV, 10 s	125 eV, 10 s	150 eV, 10 s	Data [41]	Data [42]
A_1, eV	0.71	0.50	0.56	0.67	0.77		0.4 (at 90 K)	
A_2, eV	1.18	1.18	1.18	1.18			1.36	
$A_3(E_1)$, eV		1.67	1.76	1.76	1.65	1.66	1.80	1.78
$A_{4,5}(E_2)$, eV			2.67	2.71	2.9	2.89	2.95	
$A_6(E_3)$, eV		3.34					3.40	3.23

Table 2. Parameters of nanostructures on surface and values of film band gap Bi_2Te_3

Mode of plasma treatment	25 eV, 120 s	50 eV, 40 s	100 eV, 10 s	125 eV, 10 s	150 eV, 10 s
Shape of nanostructures	Flat hillocks of triangular shaper	Pits of triangular hemisphere	Hillocks in form hemisphere	Hillocks in form hemisphere	Hillocks in form hemisphere
Height of nanostructures, nm	20	20	15	15	13
Lateral size of nanostructures, nm	25	40	20	18	17
Surface density, cm^{-2}	$(1-2)\cdot 10^{10}$	$(4-5)\cdot 10^{10}$	$(9-10)\cdot 10^{10}$	$(1-2)\cdot 10^{11}$	$(1-2)\cdot 10^{11}$
Film thickness after plasma treatment, nm	190	74	174	140	90
E_g, eV	1.15	1.06	0.87	1.29	1.28

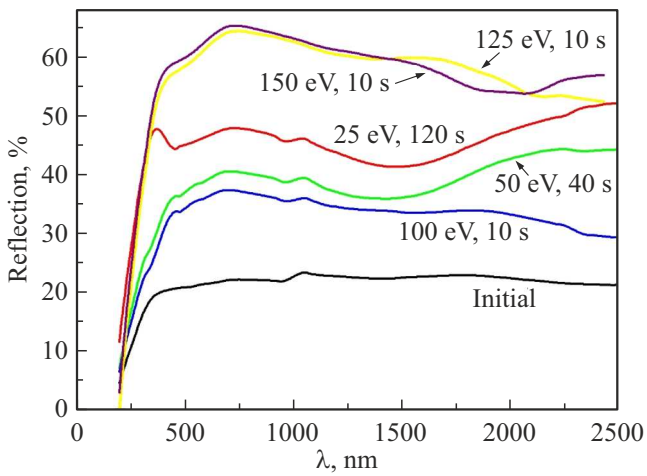

Figure 10. Spectra of specular optical reflection of films Bi_2Te_3 before and after treatment in argon plasma.

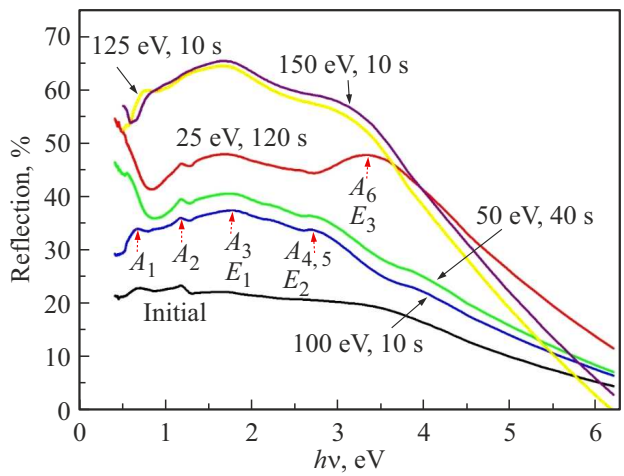

Figure 11. Spectra of specular optical reflection of films Bi_2Te_3 before and after treatment in argon plasma.

From spectral data of optical transmission (T) and reflection (R) of films Bi_2Te_3 the absorption coefficient (α) was calculated according to expression

$$\alpha = -\frac{1}{d}\ln\left(\frac{\sqrt{(1-R)^4+4T^2R^2}-(1-R)^2}{2TR^2}\right),$$

where d — sample thickness.

It is known that films Bi_2Te_3 are narrow-gap semiconductors with band gap 0.125–0.16 eV [43,44]. Hence, for initial sample of film Bi_2Te_3 in studied spectral range 200–2500 nm the edge of intrinsic absorption is not observed, and band gap can not be determined. But, for plasma treated films Bi_2Te_3 the studied spectral rage is characterized by presence of rather sharp edge of absorption

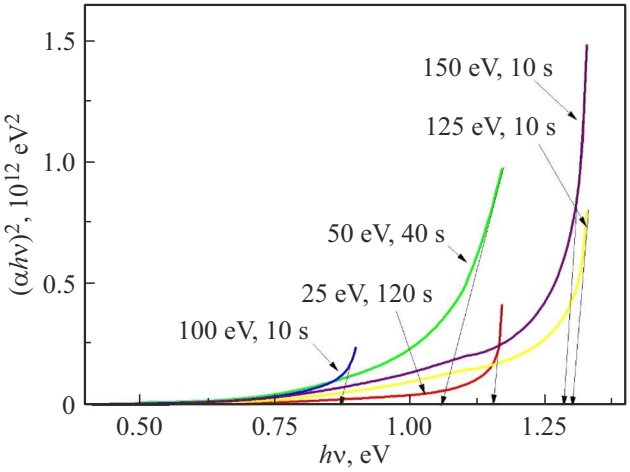

Figure 12. Spectral dependences of absorption coefficient of films Bi_2Te_3 in Tauc coordinates.

(Figure 9). Linearization of dependence $(\alpha h\nu)^2$ on $(h\nu)$ (Tauc coordinates) in region of high energy photons ensures relation of the observed absorption edge to direct allowed optical transitions. Values of the band gap of studied films E_g, determined using extrapolation of linear section of dependence $(\alpha h\nu)^2$ on $(h\nu)$ till crossing the axis of abscisses (Figure 12), are shown in Table 2.

As it follows from Table 2, the surface nanostructuring of films Bi_2Te_3 resulted in change in value of band gap. Depending on mode of plasma treatment values E_g are in range 0.87–1.29 eV. The observed significant increase in the band gap may be associated with the quantum-size effect due to the formation of nanostructures with characteristic dimensions of tens of nanometers. According to model of Al.L. Efros and A.L. Efros [45], at size of nanocrystals below Bohr radius of charge carriers, a quantum-dimensional increase in the band gap occurs. The quantum-size addition to the band gap increases inversely proportional to the square of the linear size of the nanocrystals [46]. Such effect for bismuth telluride was described in several articles [47–49]. In paper [47] for samples Bi_2Te_3, comprising spherical nanoparticles with diameter about 40 nm, we obtained value $E_g = 0.9$ eV. In paper [48] for nanoparticles Bi_2Te_3 with average diameter of 35 nm value E_g was 1.2 eV.

4. Conclusion

The study results show that ion-plasma treatment is an effective means of forming various nanostructures on the surface of epitaxial films of bismuth telluride. This is associated with high sputtering rates of layered semiconductor Bi_2Te_3 in argon plasma, this results in occurrence of large volume of „construction material“ above the film surface. and to implementation by plasma induced processes of self-formation of nanostructures of different shape and architecture. By changing the ion energy value, it became possible to vary the morphology of the nanostructured surface and obtain nanostructures of different sizes in height and in the lateral direction. Great prospects, as the first experiments show, should be expected from carrying out multi-stage treatments, which changes the course of nanostructuring processes at each new step due to the changed initial morphology of the surface. The identified effect of optical characteristics change of this films of bismuth telluride due to the formation of nanostructures on surface, comprising significant increasing of the band gap to values 0.87–1.29 eV, can be used during creation of optoelectronic systems based on Bi_2Te_3.

Acknowledgments

The authors are grateful to A.V. Epishin for assistance in conducting the studies.

Funding

The work was carried out within the framework of the state assignment of the Yaroslavl Branch of K.A. Valiev Institute of Physics and Technology of the Russian Academy of Sciences (theme No. FFNN-2022-0017) and the State Program of Scientific Research of the Republic of Belarus „Materials science, new materials and technologies“. SEM-studies are carried out in the Center of Equipment Sharing „Diagnostics of micro- and nanostructures“ under financial support from the Ministry of Education and Science of the Russian Federation.

Conflict of interest

The authors declare that they have no conflict of interest.

References

[1] B.M. Gol'tsman, V.A. Kudinov, I.A. Smirnov. Poluprovodnikovye termoelektricheskie materialy na osnove Bi_2Te_3. (Nauka, M. (1972). 320 s. (in Russian).
[2] T. Zhang, P. Cheng, X. Chen, J.-F. Jia, X.-C. Ma, K. He, L.L. Wang, H.-J. Zhang, X. Dai, Z. Fang, X.-C. Xie, Q.-K. Xue. Phys. Rev. Lett. **103**, 266803 (2009).
[3] Y.L. Chen, J.G. Analytis, J.-H. Chu, Z.K. Liu, S.-K. Mo, X.L. Qi, H.J. Zhang, D.H. Lu, X. Dai, Z. Fang, S.C. Zhang, I.R. Fisher, Z. Hussain, Z.-X. She. Science **325**, 178 (2009).
[4] D.-X. Qu, Y.S. Hor, J. Xiong, R.J. Cava, N.P. Ong. Science **329**, 821 (2010).
[5] Y. Meng, H. Zhong, Z. Xu, T. He, J.S. Kim, S. Han, S. Kim, S. Park, Y. Shen, M. Gong, Q. Xiao, S.-H. Bae. Nanoscale Horiz. **8**, 1345 (2023).
[6] J. Yao, K. Koski, W. Luo, J.J. Cha, L. Hu, D. Kong, V.K. Narasimhan, K. Huo, Y. Cui. Nature Commun. **5**, 5670 (2014).
[7] J. Liu, W. Pan, H. Wang, Z. Zhang, S. Zhang, G. Yuan, C. Yuan, Y. Ren, W. Lei. Adv. Electron. Mater. **7**, 2000851 (2021).
[8] Y. Min, G. Park, B. Kim, A. Giri, J. Zeng, J.W. Roh, S.Il. Kim, K.H. Lee, U. Jeong. ACS Nano **9**, *7*, 6843 (2015).
[9] Y.J. Lin, I. Khan, S. Saha, C.C. Wu, S.R. Barman, F.C. Kao, Z.H. Lin. Nature Commun. **12**, *1*, 180 (2021).

[10] M. Li, H.-W. Lu, S.-W. Wang, R.-P. Li, J.-Y. Chen, W.-S. Chuang, F.-S. Yang, Y.-F. Lin, C.-Y. Chen, Y.-C. Lai. Nature Commun. **13**, 938 (2022).
[11] M. Tang, J.-Y. Zhang, S. Bi, Z.-L. Hou, X.-H. Shao, K.-T. Zhan, M.-S. Cao. ACS Appl. Mater. Interfaces **11**, 33285 (2019).
[12] H. Qiao, J. Yuan, Z. Xu, C. Chen, S. Lin, Y. Wang, J. Song, Y. Liu, Q. Khan, H.Y. Hoh, C.-X. Pan, S. Li, Q. Bao. ACS Nano **9**, *2*, 1886 (2015).
[13] E.K. Belonogov, V.A. Dybov, A.V. Kostyuchenko, S.B. Kushev, D.V. Serikov, S.A. Soldatenko, M.P. Sumets. Lett. Mater. **10**, *2*, 189 (2020).
[14] Z. Yue, Q. Chen, A. Sahu, X. Wang, M.Gu. Mater. Res. Express **4**, *12*, 126403 (2017).
[15] S. Kudo, S. Tanaka, K. Miyazaki, Y. Nishi, M. Takashiri. Mater. Trans. **58**, *3*, 513 (2017).
[16] Q.-X. Guo, Z.-X. Ren, Y.-Y. Huang, Z.-C. Zheng, X.-M. Wang, W. He, Z.-D. Zhu, J. Teng. Chin. Phys. B **30**, *6*, 067307 (2021).
[17] N.I. Fedotov, A.A. Maizlakh, V.V. Pavlovskiy, G.V. Rybalchenko, S.V. Zaitsev-Zotov. Surf. Interfaces **31**, 102015 (2022).
[18] L.D. Zhaoa, B.-P. Zhang, W.S. Liu, H.L. Zhang, J.-F. Li. J. Alloys Compd. **467**, 91 (2009).
[19] I. Levchenko, K. Ostrikov. J. Phys. D **40**, *8*, 2308 (2007).
[20] I. Childres, J. Tian, I. Miotkowski, Y. Chen. Phil. Mag. **93**, *6*, 681 (2013).
[21] M. Song, J.H. Chu, J. Zhou, S. Tongay, K. Liu, J. Suh, H. Chen, J.S. Kang, X. Zou, L. You. Nanotechnology **26**, *26*, 265301 (2015).
[22] J. Jadwiszczak, D.J. Kelly, J. Guo, Y. Zhou, H. Zhang. ACS Appl. Electron. Mater. **3**, *4*, 1505 (2021).
[23] Y. You, J. Park, J. Kimz. ECS J. Solid State Sci. Technol. **12**, 075009 (2023).
[24] C.I. Fornari, P.H.O. Rappl, S.L. Morelhão, E. Abramof. J. Appl. Phys. **119**, 165303 (2016).
[25] S.L. Morelhão, S. Kycia, S. Netzke, C.I. Fornari, P.H.O. Rappl, E. Abramof. Appl. Phys. Lett. **112**, *10*, 101903 (2018).
[26] P. Ngabonziza. Nanotechnology **33**, *19*, 192001 (2022).
[27] C.I. Fornari, E. Abramof, P.H.O. Rappl, S.W. Kycia, S.L. Morelhão. MRS Adv. **5**, 1891 (2020).
[28] O. Caha, A. Dubroka, J. Humlıček, V. Holý, H. Steiner, M. Ul-Hassan, J. Sanchez-Barriga, O. Rader, T.N. Stanislavchuk, A.A. Sirenko, G. Bauer, G. Springholz. Crystal Growth & Design **13**, *8*, 3365 (2013).
[29] H. Steiner, V. Volobuev, O. Caha, G. Bauer, G. Springholz, V. Holý. J. Appl. Cryst. **47**, 1889 (2014).
[30] Y. Tanaka, Y. Krockenberger, Y. Kunihashi, H. Sanada, H. Omi, H. Gotoh, K. Oguri. Appl. Phys. Express **15**, *6*, 065502 (2022).
[31] Y. Nie, A.T. Barton, R. Addou,Y. Zheng, L.A. Walsh, S.M. Eichfeld, R. Yue, C. Cormier, C. Zhang, Q. Wang, C. Liang, J.A. Robinson, M. Kim, W. Vandenberghe, L. Colombo, P.-R. Cha,R.M. Wallace, C.L. Hinkle, K. Cho. Nanoscale **10**, *31*, 15023 (2018).
[32] S. Zimin, E. Gorlachev, I. Amirov. Inductively Coupled Plasma Sputtering: Structure of IV−VI Semiconductors. In: Encyclopedia of Plasma Technology. 1st ed. CRC Press, N.Y. (2017). P. 679−691. https://doi.org/10.1081/E-EPLT-120053966 https://www.routledgehandbooks.com/doi/10.1081/E-EPLT-120053966
[33] S.P. Zimin, I.I. Amirov, M.S. Tivanov, N.N. Kolesnikov, O.V. Korolik, L.S. Lyashenko, D.V. Zhyhulin, L.A. Mazaletskiy, S.V. Vasilev, O.V. Savenko. Phys. Solid State **65**, *4*, 671 (2023).
[34] G. Hao, X. Qi, L. Yang, Y. Liu, J. Li, L. Ren, F. Sun, J. Zhong. AIP Adv. **2**, *1*, 012114 (2012).
[35] Y. Zhao, M. de la Mata, R.L.J. Qiu, J. Zhang, X. Wen, C. Magen, X.P.A. Gao, J. Arbiol, Q. Xiong. Nano Res. **7**, *9*, 1243 (2014).
[36] W. Lu, Y. Ding, Y. Chen, Z.L. Wang, J. Fang. J. Am. Chem. Soc. **127**, *28*, 10112 (2005).
[37] Y. Hosokawa, K. Tomita, M. Takashiri. Sci. Rep. **9**, 10790 (2019).
[38] P. Sigmund. Elements of sputtering theory. In: Nanofabrication by Ion-Beam Sputtering / Eds T. Som, D. Kanjilal. Pan Stanford Publishing (2013). P. 1−40. https://doi.org/10.4032/9789814303767
[39] W. Richter, C.R. Becker. Phys. Status Solidi B **84**, 619 (1977).
[40] W. Kullmann, J. Geurts, W. Richter, N. Lehner, H. Rauh, U. Steigenberger, G. Eichhorn, R. Geick. Phys. Status Solidi B **125**, 131 (1984).
[41] V.V. Sobolev, S.D. Shutov, Y.V. Popov, S.N. Shestatskii. Phys. Status Solidi B **30**, 349 (1968).
[42] D.L. Greenaway, G. Harbeke. J. Phys. Chem. Solids **26**, *10*, 1585 (1965).
[43] P. Pecheur, G. Toussaint. Phys. Lett. A **135**, *3*, 223 (1989).
[44] I.G. Austin. Proc. Phys. Soc. **72**, *4*, 545 (1958).
[45] Al.L. Efros, A.L. Efros. FTP **16**, *7*, 1209 (1982). (in Russian).
[46] I.E. Tyschenko, V.A. Volodin. FTP **46**, *10*, 1309 (2012). (in Russian).
[47] Y. Saberi, S.A. Sajjadi, H. Mansouri. J. Mater. Sci.: Mater. Electron. **31**, 18988 (2020).
[48] P. Srivastava, K. Singh. J. Exp. Nanosci. **9**, *10*, 1064 (2014).
[49] J. Dheepa, R. Sathyamoorthy, S. Velumani. Mater. Charact. **58**, *8−9*, 782 (2007).

Translated by I.Mazurov